Letter

Pauli blockade catalogue and three- and four-particle Kondo effect in bilayer graphene quantum dots

Chuyao Tong [1,*], Annika Kurzmann,[1,2] Rebekka Garreis [1], Kenji Watanabe,[3] Takashi Taniguchi,[4]
Thomas Ihn,[1] and Klaus Ensslin [1]

[1]*Solid State Physics Laboratory, ETH Zurich, CH-8093 Zurich, Switzerland*

[2]*2nd Institute of Physics, RWTH Aachen University, Aachen 52074, Germany*

[3]*Research Center for Functional Materials, National Institute for Materials Science, 1-1 Namiki, Tsukuba 305-0044, Japan*

[4]*International Center for Materials Nanoarchitectonics, National Institute for Materials Science, 1-1 Namiki, Tsukuba 305-0044, Japan*

Pauli blockade is a fundamental quantum phenomenon that also serves as a powerful tool for qubit manipulation and readout. While most systems exhibit a simple even-odd pattern of double-dot Pauli spin blockade due to the preferred singlet pairing of spins, the additional valley degree of freedom offered by bilayer graphene greatly alters this pattern. Inspecting bias-triangle measurements at double-dot charge degeneracies with up to four electrons in each dot reveals a much richer double-dot Pauli blockade catalog with both spin and/or valley blockade. In addition, we use single-dot Kondo effect measurements to substantiate our understanding of the three- and four-particle state spectra by analyzing their magnetic field dependence. With high controllability and reported long valley- and spin-relaxation times, bilayer graphene is a rising platform for hosting semiconductor quantum dot qubits. A thorough understanding of state spectra is crucial for qubit design and manipulation, and the rich Pauli blockade catalog provides an abundance of qubit operational possibilities and opportunities to explore intriguing spin and valley physics.

Carbon-based materials are promising hosts for spin qubits [1–4] due to the natural abundance of 98.9% low-mass, nuclear-spin free ^{12}C. Experimental advancements achieved in recent years [5–21] have demonstrated the great potential for electrostatically defined bilayer graphene (BLG) quantum dots (QDs) to host spin and valley qubits, with highly tunable QDs' geometry and tunnel couplings, as well as gate-tunable valley *g*-factors [9], and reported remarkably long valley-relaxation time $T_1 > 500$ ms [20], and spin-relaxation times T_1 up to 50 ms [16,17,20], comparable with the state-of-the-art results achieved in other semiconductor quantum dot systems [22].

To harvest the full potential of BLG QDs, a thorough understanding of the relevant QD state spectra is essential. In BLG, in addition to spins, up and down, there exist two valleys, K^+ and K^-, which couple to an external perpendicular magnetic field due to their nontrivial Berry curvature [5,9,10,23,24]. These valleys enrich the spectra of BLG, and lead to intriguing properties, such as the spin-triplet valley-singlet single-dot two-particle ground state [11,18,25,26] and the double-dot two-carrier Pauli spin- and valley-blockade [15]. Most other systems, i.e., systems without valleys, exhibit

no Pauli blockade when an *odd* number of carriers reside in a double dot due to the preferred singlet pairing of spins [27–32]. In contrast, in BLG three-carrier spin blockade has been demonstrated recently [19].

Not limited to three carriers, the entire double-dot Pauli blockade catalog with up to four carriers (i.e., a full shell) in each dot is far richer for BLG than for a conventional system. Our main result is summarized in Fig. 1(a), a comparison of schematic double-dot charge stability diagrams for (i) BLG and for (ii) a conventional system. In a conventional system, an even-odd pattern of Pauli spin-blocked and nonblocked transitions arise [32]; in contrast, in BLG Pauli blockade could arise from both spin *and* valley selection rules. The rich blockade structure provides a multitude of qubit operational positions, allowing us to exploit the unique spin and valley physics for varied qubit manipulation and control [33].

In this work, we study transport measurements through BLG double quantum dot (DQD). By analyzing finite-bias triangles at various charge degeneracies, we discuss the states and transitions involved, and hence the nature of the observed Pauli blockade as summarized in Fig. 1(a), going beyond the previously discussed two-carrier [15] and three-carrier [19] cases. Substantiating our understanding of the three- and four-particle state spectra experimentally, we further present transport measurements through a single BLG QD, probing the magnetic field dependence of the state spectra with the Kondo effect (similar to Ref. [12]).

The BLG QDs are defined electrostatically [device shown in Fig. 1(b)]. We use the band gap arising from a perpendicular displacement field [34–36], achieved by the global back gate

---

*ctong@phys.ethz.ch
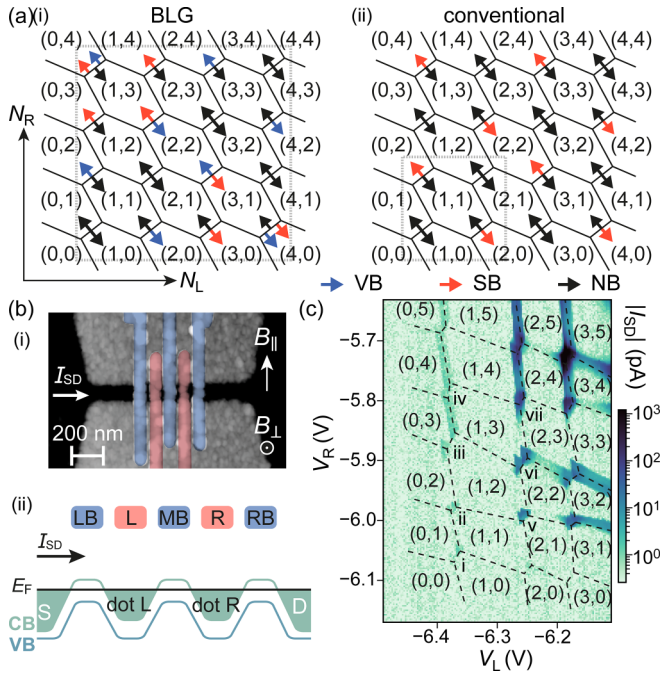
FIG. 1. (a) Schematic double-dot charge stability diagram for (i) BLG and (ii) a conventional system [32]. Nonblocked (NB), spin-blocked (SB), and valley-blocked (VB) transitions are marked with black, red, and blue arrows. (b)(i) False-colored AFM image of the device. (ii) Conduction band (CB) and valence band (VB) edge variation along the channel. Dots L and R are formed underneath the respective plunger gates (red), with gate voltages V_L and V_R. Left-barrier (LB), middle-barrier (MB), and right-barrier (RB) gates (blue) control the respective tunnel barriers. (c) Double-dot charge stability map at $V_{SD} = 1.5$ mV with stable charge states marked in the respective Coulomb-blockaded regions and separated with dashed lines. Roman numerals label the triple points studied in this work, with zoom-ins presented in Fig. 2(b). The number of electrons in the left N_L and in the right N_R dot increase from left to right, and from top to bottom.

and various local top gates. The split gates [Fig. 1(b,i), gray] form a one-dimensional (1D) channel. Another layer of gates (red and blue) locally tune the potential landscape within this channel. See Supplemental Materials S1 [37] for more detail.

We form an electron DQD with *n*-type leads and tunable tunnel barriers [potential landscape depicted in Fig. 1(b,ii)]. The plunger gate voltages V_L and V_R define dots L and R underneath the respective gates (red). More negative V_L and V_R deplete the respective dot discretely to the last electron. When a voltage V_{SD} is applied between the source and drain leads, finite-bias triangles form at triple-points where three charge configurations coexist. The distinctive honeycomb pattern of the double-dot charge stability diagram is observed on Fig. 1(c). Charging energies $\sim 6-10$ meV are estimated for both dots, much larger than the energy scales that will be considered in the following discussions.

The nature of Pauli blockade is determined by the relevant spin and valley states involved. Understanding the blockade therefore demands a discussion on the single-dot *N*-particle state spectra [sketched in Fig. 2(a)]. We choose to discuss the states first with the single-particle notation:

One particle: The fourfold spin and valley states are split by a small $(60-80\,\mu eV)$ Kane-Mele [12,13,38] spin-orbit gap Δ_{SO} into two Kramer pairs: lower-energy $\downarrow K^-$ and $\uparrow K^+$, and higher-energy $\downarrow K^+$ and $\uparrow K^-$. At zero field, Δ_{SO} quantizes the spins and valleys along the direction perpendicular to the BLG sheet.

Two particles: The spin-triplet valley-singlet is the ground state, as shown in Refs. [11,18,25,26] and Fig. 2(a,ii).

Three particles: Taking three of the four available states for one particle gives us the spectrum shown in Fig. 2(a,iii), with Kramer pairs $\downarrow K^- \uparrow K^+ \downarrow K^+$ and $\downarrow K^- \uparrow K^+ \uparrow K^-$ lower, and $\downarrow K^+ \uparrow K^- \downarrow K^-$ and $\downarrow K^+ \uparrow K^- \uparrow K^+$ higher in energy.

Four particles: Four carriers complete the shell, occupying all the available states in the lowest-energy orbital.

Alternative to the single-particle notation, we can also write the states with their quantum numbers: the total spin (valley) number σ (τ), and their projections to the spin (valley) quantization axis σ_z (τ_z). We define $\sigma_z = \pm 1/2$ for spins $\uparrow / \downarrow$, and $\tau_z = \pm 1/2$ for valleys $K^\pm$. This notation $|\sigma, \sigma_z; \tau, \tau_z\rangle$ is marked in Fig. 2(a) for the ground states at zero magnetic fields (black). The valley quantization axis is always out of plane, whereas the spin quantization axis is out of plane at zero *B*-field due to Δ_{SO} [12,13], and tilts towards in-plane in external $B_\parallel$. A *B*-field applied in any direction shifts spin-state energies by $\sigma_z g_s \mu_B B$, while only an out-of-plane field shifts the valley-state energies by $\tau_z g_v \mu_B B_\perp$, where μ_B is the Bohr magneton, $g_s = 2$ the spin *g*-factor [5,10,11], and $g_v \gg g_s$ the gap-size and dot-geometry dependent valley *g*-factor [9,12].

Since the interdot coupling is weak, we can choose to write the double-dot states as product states of the single-dot states in the left and in the right dot, written in a bracket $(|N_L\rangle, |N_R\rangle)$. The spin (valley) projection of a double-dot state is thus simply the sum of its constituting single-dot states $\sigma_z = \sigma_{z,NL} + \sigma_{z,NR}$ ($\tau_z = \tau_{z,NL} + \tau_{z,NR}$). Since both spin-orbit [38,39] and valley-orbit [40] effects are weak in BLG, we assume that tunneling conserves all the spin and valley numbers. Transitions between double-dot charge configurations are *not* blocked only if, for every degenerate ground state of the initial charge configuration, there exists a state in the final charge configuration being lower in energy and matching all quantum numbers with the initial state. Otherwise, some form of Pauli blockade arises; its nature depends on the mismatched quantum number (spin and/or valley).

In Fig. 2(b), we present zoom-ins of the finite-bias triangles labeled with Roman numerals i–vii in Fig. 1(c). The barrier gate voltages are adjusted slightly such that the dot geometry and tunnel couplings are similar for different charge transitions. Charge-configuration transitions (dashed arrows) can be nonblocked (black), spin blocked (red), or valley blocked (blue):

(i) *(1,0)–(0,1)*: Any loaded electron hops between the two dots with the same one-particle states. No blockade is observed: the bias triangles are complete for both bias directions.

(ii) *(1,1)–(0,2)*: Studied in Ref. [15], the system is stuck when a (1,1) state with $\tau_z = \pm 1$ (valley-polarized state, e.g., K^- in both dots) is loaded, as transition to the (0,2) ground state with $\tau_z = 0$ (paired valley singlet S_v) is forbidden by valley conservation. The valley-blocked transition $(1,1) \rightarrow$
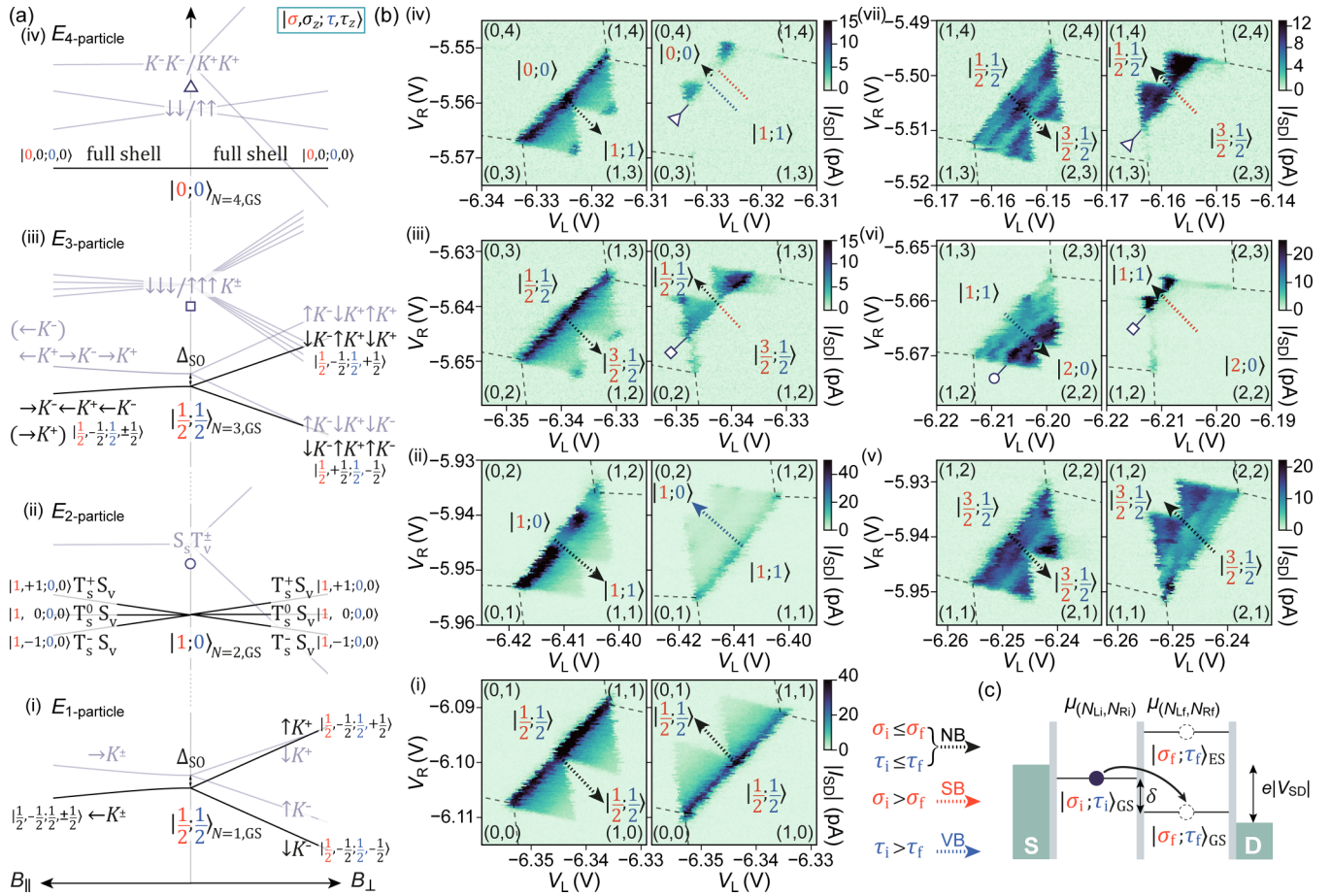
FIG. 2. (a) N-particle state spectra E_N with zero-field ground states (black) and relevant excited states (gray) in in-plane $B_\parallel$ and out-of-plane $B_\perp$ magnetic field, for [(i)–(iv)] $N = 1-4$. The zero-field N-particle ground state is labeled as $|\sigma;\tau\rangle_{N,GS}$, where σ (red) and τ (blue) is its total spin and valley number. (b) Finite-bias triangles at $V_{SD} = -1$ mV (left panel) and $+1$ mV (right panel), at charge degeneracies (i) (0,1)–(1,0), (ii) (0,2)–(1,1) (reproduced from Supplemental Material of Ref. [15]), (iii) (0,3)–(1,2) (reproduced from Ref. [19]), (iv) (0,4)–(1,3), (v) (1,2)–(2,1), (vi) (1,3)–(2,2), and (vii) (1,4)–(2,3). Arrows mark the direction of charge configuration transitions; nonblocked (NB), spin-blocked (SB), and valley-blocked (VB) transitions are marked with black, red, and blue arrows, respectively. Ground states of each charge configuration are labeled as $|\sigma = \sigma_{NL} + \sigma_{NR}; \tau = \tau_{NL} + \tau_{NR}\rangle$. (c) Schematic illustrating the condition of Pauli blockade, determined by the total spin (valley) number of the ground states of the initial σ_i (τ_i) and final σ_f (τ_f) charge configuration.

(0, 2) suppresses the current in the bias triangles [right, Fig. 2(b,ii)], as compared to the nonblocked ones (left).

(iii) *(1,2)–(0,3):* Studied in Ref. [19], transition $(1, 2) \to (0, 3)$ is spin blocked; the system is stuck in the maximally spin-polarized (1,2) states $\sigma_z = \pm 3/2$ [e.g., $(\downarrow, T_s^-)$], since the (0,3) ground state can only offer $\sigma_z = \pm 1/2$ states [41,42]. Current in the $(1, 2) \to (0, 3)$ bias triangles [right, Fig. 2(b,iii)] is therefore strongly suppressed, as compared to the nonblocked $(0, 3) \to (1, 2)$ ones (left). The spin-blockade current suppression is stronger here than that of valley blockade in (ii). Marked by a square at detuning ~ 0.6 meV, transport resumes when the (0,3) excited state with $\sigma_z = \pm 3/2$ [$(0, \downarrow\downarrow\downarrow / \uparrow\uparrow\uparrow)$, Fig. 2(a,iii) gray] becomes lower in energy than the (1,2) ground state.

(iv) *(1,3)–(0,4):* Transition $(0, 4) \to (1, 3)$ is nonblocked, where $(1, 3) \to (0, 4)$ is both spin *and* valley blocked with strong current suppression: The (1,3) ground state can be spin ($\sigma_z = \pm 1$) or valley ($\tau_z = \pm 1$) polarized, whereas (0,4) only accepts a spin *and* valley paired full shell. The blockade lifts (indicated by the triangle) when the polar-

ized (0,4) excited state with $\sigma_z = \pm 1$ $(0, \downarrow\downarrow / \uparrow\uparrow)$ or $\tau_z \pm 1$ $(0, K^-K^-/K^+K^+)$ [gray in Fig. 2(a,iv)] becomes accessible at detuning ~ 0.8 meV.

(v) *(2,1)–(1,2):* Since the states in the two charge configurations are essentially the same with only the roles of the left and the right dot switched, no blockade exists in either direction.

(vi) *(2,2)–(1,3):* Both sets of bias triangles in Fig. 2(b,vi) show regions with current suppression, with spin blockade (right) stronger than valley blockade (left). For $(2, 2) \to (1, 3)$, a fully spin-polarized (2,2) ground state with $\sigma_z = \pm 2$, e.g., $(T_s^- S_v, T_s^- S_v)$, is blocked to the (1,3) ground state where the maximally spin-polarized state has only $\sigma_z = \pm 1$, e.g., $(\downarrow K^-, \downarrow K^- \uparrow K^+ \downarrow K^+)$. This spin blockade is lifted (marked by the square) upon accessing the spin-polarized excited three-particle states $\downarrow\downarrow\downarrow / \uparrow\uparrow\uparrow$ in the right dot [gray in Fig. 2(a,iii)]. For $(1, 3) \to (2, 2)$, a valley-polarized (1,3) ground state with $\tau_z = \pm 1$, e.g., $(\downarrow K^-, \downarrow K^- \uparrow K^+ \uparrow K^-)$, is blocked to the (2,2) ground state that allows only fully paired valleys $(T_s S_v, T_s S_v)$ with $\tau_z = 0$. This valley blockade is lifted
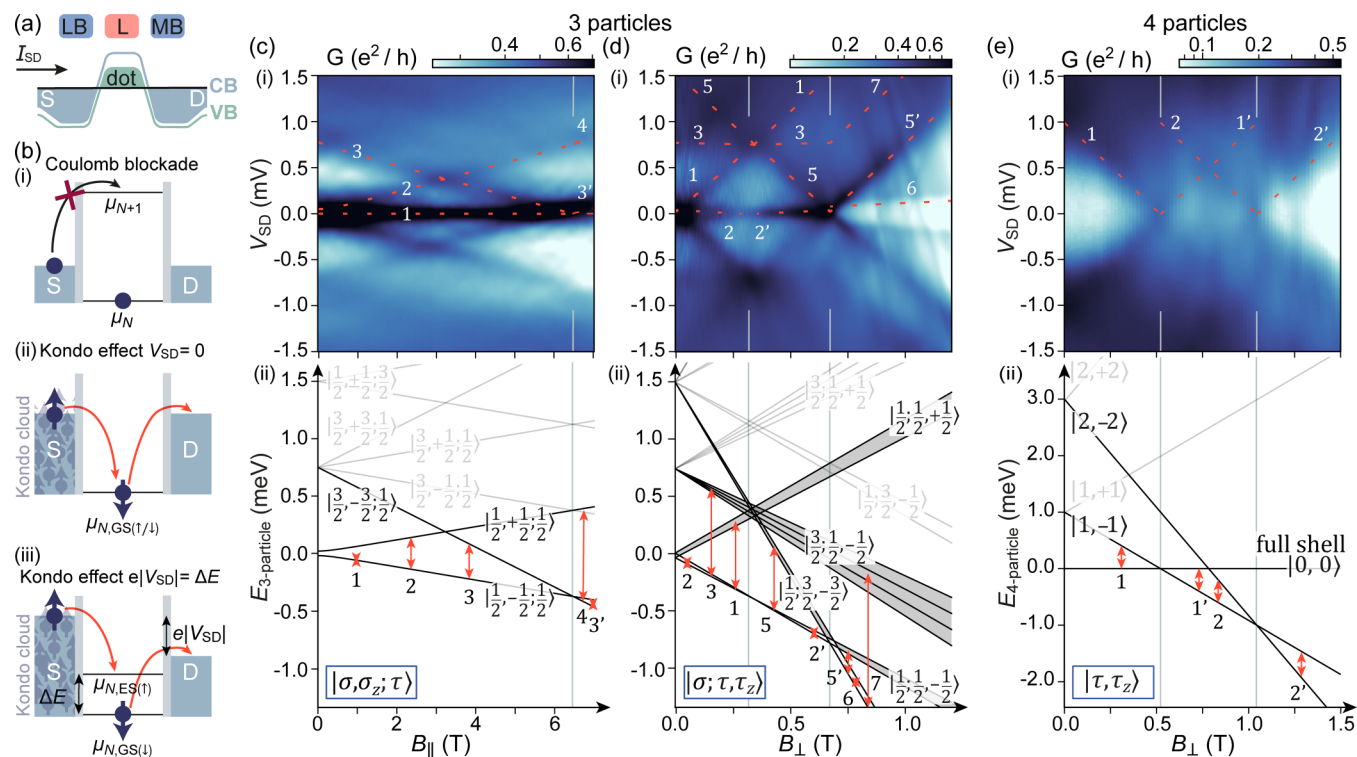
FIG. 3. (a) Potential landscape along the channel for the single hole dot. (b) Schematics of (i) Coulomb blockade, (ii) Kondo-assisted spin-flip co-tunnelings involving degenerate ground states with different quantum numbers at $V_{SD} = 0$, and (iii) involving the ground and an excited state at $V_{SD} = \Delta E$, conserving energies. [(c)–(e)] (i) Evolution of conductance along finite bias cuts at fixed V_L for (c) three holes in in-plane field $B_{\parallel}$, (d) three holes in out-of-plane field $B_{\perp}$, and (e) four holes in out-of-plane field $B_{\perp}$, with (ii) respectively deduced three- and four-particle level spectra and relevant co-tunneling transitions. States are labeled with total spin (valley) numbers σ (τ), and projected spin (valley) numbers σ_z (τ_z).

(marked by the circle) upon accessing the valley-polarized excited two-particle states $S_sT^{\pm}$ [gray in Fig. 2(a,ii)] in either dot. Here, transitions in both directions are Pauli blocked but for different quantum numbers—an intriguing situation special to BLG.

(vii) *(1,4)–(2,3)*: The transition $(2, 3) \rightarrow (1, 4)$ is spin blocked and $(1, 4) \rightarrow (2, 3)$ nonblocked, demonstrated by the strong current suppression in the right bias triangles as compared to the left ones in Fig. 2(b,vii). The $(1, 4)$ state, a full shell in the right dot and a single electron in the left dot, cannot accommodate the maximally spin-polarized $(2,3)$ state with $\sigma_z = \pm 3/2$, e.g., $(T_s^- S_v, \downarrow K^- \uparrow K^+ \downarrow K^+)$. The spin blockade lifts (marked by the triangle) upon accessing the spin-polarized four-particle excited state $\downarrow\downarrow / \uparrow\uparrow$ [gray in Fig. 2(a,iv)] in the right dot.

The nature of Pauli blockade at various charge transitions is summarized in Fig. 1(a) and compared with the conventional case where levels are filled with alternating spins. The richer structure in BLG stems from (1) the additional valley degrees of freedom, and as a result (2) the single-dot two-particle ground state being a spin triplet [11,18] instead of a spin singlet.

From the above discussion, we see that the maximally spin-(valley-)polarized [i.e., with maximum $|\sigma_z|$ ($|\tau_z|$)] double-dot ground state of a charge configuration is responsible for spin (valley) blockade. The maximum $|\sigma_z|$ ($|\tau_z|$) can be found by simply summing the total spin (valley) quantum number of the left and right single-dot ground states $\sigma_{NL} + \sigma_{NR}$ ($\tau_{NL} + \tau_{NR}$).

We can therefore summarize the above discussion into a simpler rule [illustrated in Fig. 2(c)]: If the total spin (valley) number of the double-dot ground state of the final charge configuration σ_f (τ_f) is lower than that of the initial charge configuration σ_i (τ_i), then there are (at least) initial states with $\sigma_z = \pm\sigma_i$ ($\tau_z = \pm\tau_i$) that do not exist in the final ground states, and this transition is spin (valley) blocked.

To substantiate the proposed three- and four-particle state spectra in Fig. 2(a) that form the basis of the double-dot Pauli blockade analysis, we present experimental data investigating the spectra in magnetic field with the single-dot Kondo effect [43], similar to the analysis performed in Ref. [12].

With V_L as the plunger gate voltage, we tune the system to a single hole dot (the electron and hole spectra in BLG have so far been found identical) with strong dot-lead tunnel coupling, allowing for the observation of the Kondo effect [12,43] [sketched in Fig. 3(a), see Supplemental Materials S1 [37] for details].

The Coulomb blockade in a QD [Fig. 3(b,i)] can be lifted by the Kondo effect [Fig. 3(b,ii)] [43–48], allowing for finite conductance G: the unpaired spin (valley) state in the dot attracts a cloud of carriers with opposite spins (valleys) to the strongly coupled lead, assisting spin- (valley-)flip co-tunneling events [12]. For energy conservation, the energy gained by the carrier escaping the dot equates to the energy lost by the carrier entering simultaneously from the lead. Therefore, a conductance resonance around zero V_{SD} indicates the existence of degenerate N-particle ground states with

different spin (valley) quantum numbers, as observed in the Coulomb diamonds in Fig. S1 for one, two, and three holes. The absence of this resonance for four holes confirms the formation of a singly degenerate full shell with paired spins and valleys. At finite V_{SD}, co-tunnelings with excited states become possible [Fig. 3(b,iii)]. Conductance resonances occur when $e|V_{\mathrm{SD}}| = \mu_{N,\mathrm{ES}} - \mu_{N,\mathrm{GS}} := \Delta E$, i.e., when the bias provides exactly the energy difference between the states. From the Coulomb diamonds in Fig. S1 we obtain charging energies ~ 4 meV, larger than the energy scales in the following discussions.

Fixing V_{L} for three and four holes (See Supplemental Materials. S1 [37] for the corresponding Coulomb diamonds and the chosen V_{L}), we apply external in-plane $B_{\parallel}$ and out-of-plane $B_{\perp}$ field which shift the energies of spin and valley states. Slopes of conductance resonances in B-fields offer information on the character of the states: a slope of $\pm g_{\mathrm{s}}$ ($\pm g_{\mathrm{v}}$), corresponds to a spin- (valley-) flip co-tunneling transition between the ground state and an excited state with different spin (valley) numbers $\Delta \sigma_z = \pm 1$ ($\Delta \tau_z = \pm 1$). For the discussion of the Kondo effect, we label the single QD states exclusively with spin and valley numbers for compactness. We discuss for positive V_{SD} only, though the physics is equivalent for negative V_{SD}.

With these rules in mind, we first look at conductance maps Fig. 3(c,i) for three particles in in-plane magnetic field, which couple only to spins but not to valleys. We thus see resonance 1 at zero-bias corresponding to valley-flip co-tunnelings, indicating the ground-state valley degeneracy $\tau_z = \pm 1/2$. Resonance 2 splits off from 1 with slope $+g_{\mathrm{s}} \approx 2$, indicating spin-flip co-tunnelings and thus the zero-field spin degeneracy of the ground state $\sigma_z = \pm 1/2$. Starting from 0.7 mV at $B_{\parallel} = 0$, resonance 3 shows a slope of $-g_{\mathrm{s}} \approx 2$, indicating spin-flip co-tunnelings between the ground state with $\sigma_z = -1/2$ and an excited state with lower spin number. This maximally spin-polarized three-particle state with $\sigma_z = -3/2$ appears as an excited state at 0.7 meV as it requires contributions of an excited orbital level. This state is also responsible for lifting the $(1,2) \rightarrow (0,3)$ and $(2,2) \rightarrow (1,3)$ spin blockade [Figs. 2(b,iii) and 2(vi), squares, also sketched in Fig. 2(a,iii)]. This excited state becomes the ground state at $B_{\parallel} > 7$ T. Co-tunneling events then arise from this state.

In out-of-plane field [Fig. 3(d)], as $g_{\mathrm{v}} \gg g_{\mathrm{s}}$ we resolve mainly valley splitting. The nonresolved spin-multiplet bundles are colored gray together. Being a zero-bias resonance in $B_{\parallel}$, resonance 1 splits off in $B_{\perp}$ with $g_{\mathrm{v}} \approx 40$, corresponding to valley-flip co-tunnelings. We observe a "focusing" effect of resonance 2 becoming the narrowest at 0.35 ± 0.10 T, arising from the competition between the zero-field splitting Δ_{SO} [12,13] and the Zeeman splitting, changing the ground state from $\sigma_z = 1/2; \tau_z = -1/2$ to $\sigma_z = -1/2; \tau_z = -1/2$. With $g_{\mathrm{s}} = 2$ we estimate $\Delta_{\mathrm{SO}} \approx 40 \pm 10$ μeV, slightly lower than that reported for one-particle states [12,13,19]. Starting from 1.5 mV at $B_{\perp} = 0$, resonance 5 with $g \sim 40$ corresponds to valley-flip co-tunnelings between the ground state with $\tau_z = -1/2$ and an excited state with lower valley number $\tau_z = -3/2$. Since there exists no resonance with a slope of $g \sim -40$ starting from 0.7 mV at $B_{\perp} = 0$, we conclude that the $\sigma_z = -3/2$ excited states contain no $\tau_z = -3/2$ states. At $B_{\perp} > 0.7$ T, the valley-polarized $\tau_z =$

$-3/2$ state becomes the ground state. From there resonance 6 with $g_{\mathrm{s}} = +2$ corresponds to spin-flip co-tunnelings between the $\tau_z = -3/2; \sigma_z \pm 1/2$ states. Resonances 5' and 7 with slopes $g \sim +40$ correspond to valley-flip co-tunnelings of the $\tau_z = -3/2$ ground state with the spin-doublet of $\sigma = 1/2; \tau = 1/2, \tau_z = -1/2$, and with the quadruplet bundle of $\sigma = 3/2; \tau = 1/2, \tau_z = -1/2$, respectively.

It is worth noting that the three-particle $\sigma_z = 3/2$ state is lower in energy (~ 0.7 meV) than the $\tau_z = 3/2$ state (~ 1.5 meV), similar to the two-particle case [11,18] where, counterintuitively, the spin triplet ($\sigma = 1$) is the ground state while the valley triplet ($\tau = 1$) is the excited state.

We now turn our attention to four-particle states in out-of-plane field. Intuitively, the four-hole ground state is a full shell with degeneracy of 1, and indeed no zero-bias peak occurs at zero field. Starting at 1 mV, resonance 1 shows $g_{\mathrm{v}} \sim -40$, corresponding to valley-flip co-tunnelings between the full shell and an excited state with $\tau_z = -1$. This state becomes the ground state at $B_{\perp} > 0.5$ T. At $B_{\perp} > 1.1$ T, a fully valley-polarized state with $\tau_z = -2$ becomes the ground state. Resonances 2 and 2' arise from co-tunnelings between the $\tau_z = -2$ and the $\tau_z = -1$ states. Tracing resonance 2 back to $B_{\perp} = 0$, we obtain energy of the $\tau_z = -2$ excited state ~ 3 meV.

The excited states are higher in energy due to involvement of higher orbital levels. Their energy deduced from the Kondo measurements agrees well with that deduced from lifting of the double-dot blockade (Fig. 2), which also agrees qualitatively with the calculated orbital levels [25,26].

As the ground states change in B field, the double-dot Pauli blockade also changes in nature. For charge degeneracies (1,2)–(0,3), (1,3)–(0,4), and (2,2)–(1,3), we study conductance along the detuning axis of bias triangles in $B_{\perp}$ (see Supplemental Materials S2 [37]). The magnetospectroscopy shows the evolution of Pauli blockade in $B_{\perp}$, and agrees with the suggested [Fig. 2(a)] and demonstrated [Figs. 3(c)–3(e)] N-particle state spectra.

To conclude, we established three- and four-particle state spectra in BLG QDs by examining their magnetic field dependence with the Kondo effect. By discussing the relevant N-particle states and inspecting the double-dot bias-triangle measurements between a multitude of charge configurations, we reveal the Pauli blockade catalog for BLG QDs as summarized in Fig. 1(c,i), notably richer and intriguingly different compared to the canonical spin blockade [32] [Fig. 1(c,ii)]. The rich BLG state spectra and Pauli blockade catalog offer an abundance of different qubit operational positions, allowing for improved qubit manipulation and control exploiting unique spin and valley properties.

[1] B. Trauzettel, D. V. Bulaev, D. Loss, and G. Burkard, Spin qubits in graphene quantum dots, Nat. Phys. **3**, 192 (2007).

[2] R. Hanson, L. P. Kouwenhoven, J. R. Petta, S. Tarucha, and L. M. K. Vandersypen, Spins in few-electron quantum dots, Rev. Mod. Phys. **79**, 1217 (2007).

[3] X. Liu and M. C. Hersam, 2D materials for quantum information science, Nat. Rev. Mater. **4**, 669 (2019).

[4] F.-M. Jing, Z.-Z. Zhang, G.-Q. Qin, G. Luo, G. Cao, H.-O. Li, X.-X. Song, and G.-P. Guo, Gate-controlled quantum dots based on 2D materials, Adv. Quantum Technol. **5**, 2100162 (2022).

[5] M. Eich, F. Herman, R. Pisoni, H. Overweg, A. Kurzmann, Y. Lee, P. Rickhaus, K. Watanabe, T. Taniguchi, M. Sigrist, T. Ihn, and K. Ensslin, Spin and valley states in gate-defined bilayer graphene quantum dots, Phys. Rev. X **8**, 031023 (2018).

[6] M. Eich, R. Pisoni, A. Pally, H. Overweg, A. Kurzmann, Y. Lee, P. Rickhaus, K. Watanabe, T. Taniguchi, K. Ensslin *et al.*, Coupled quantum dots in bilayer graphene, Nano Lett. **18**, 5042 (2018).

[7] L. Banszerus, B. Frohn, A. Epping, D. Neumaier, K. Watanabe, T. Taniguchi, and C. Stampfer, Gate-defined electron–hole double dots in bilayer graphene, Nano Lett. **18**, 4785 (2018).

[8] A. Kurzmann, H. Overweg, M. Eich, A. Pally, P. Rickhaus, R. Pisoni, Y. Lee, K. Watanabe, T. Taniguchi, T. Ihn, and K. Ensslin, Charge detection in gate-defined bilayer graphene quantum dots, Nano Lett. **19**, 5216 (2019).

[9] C. Tong, R. Garreis, A. Knothe, M. Eich, A. Sacchi, K. Watanabe, T. Taniguchi, V. Fal'ko, T. Ihn, K. Ensslin *et al.*, Tunable valley splitting and bipolar operation in graphene quantum dots, Nano Lett. **21**, 1068 (2021).

[10] R. Garreis, A. Knothe, C. Tong, M. Eich, C. Gold, K. Watanabe, T. Taniguchi, V. Fal'ko, T. Ihn, K. Ensslin, and A. Kurzmann, Shell filling and trigonal warping in graphene quantum dots, Phys. Rev. Lett. **126**, 147703 (2021).

[11] A. Kurzmann, M. Eich, H. Overweg, M. Mangold, F. Herman, P. Rickhaus, R. Pisoni, Y. Lee, R. Garreis, C. Tong, K. Watanabe, T. Taniguchi, K. Ensslin, and T. Ihn, Excited states in bilayer graphene quantum dots, Phys. Rev. Lett. **123**, 026803 (2019).

[12] A. Kurzmann, Y. Kleeorin, C. Tong, R. Garreis, A. Knothe, M. Eich, C. Mittag, C. Gold, F. K. de Vries, K. Watanabe *et al.*, Kondo effect and spin–orbit coupling in graphene quantum dots, Nat. Commun. **12**, 6004 (2021).

[13] L. Banszerus, S. Möller, C. Steiner, E. Icking, S. Trellenkamp, F. Lentz, K. Watanabe, T. Taniguchi, C. Volk, and C. Stampfer, Spin-valley coupling in single-electron bilayer graphene quantum dots, Nat. Commun. **12**, 5250 (2021).

[14] L. Banszerus, A. Rothstein, T. Fabian, S. Möller, E. Icking, S. Trellenkamp, F. Lentz, D. Neumaier, K. Watanabe, T. Taniguchi *et al.*, Electron–hole crossover in gate-controlled bilayer graphene quantum dots, Nano Lett. **20**, 7709 (2020).

[15] C. Tong, A. Kurzmann, R. Garreis, W. W. Huang, S. Jele, M. Eich, L. Ginzburg, C. Mittag, K. Watanabe, T. Taniguchi *et al.*, Pauli blockade of tunable two-electron spin and valley states in graphene quantum dots, Phys. Rev. Lett. **128**, 067702 (2022).

[16] L. M. Gächter, R. Garreis, J. D. Gerber, M. J. Ruckriegel, C. Tong, B. Kratochwil, F. K. de Vries, A. Kurzmann, K. Watanabe, T. Taniguchi *et al.*, Single-shot spin readout in graphene quantum dots, PRX Quantum **3**, 020343 (2022).

[17] L. Banszerus, K. Hecker, S. Möller, E. Icking, K. Watanabe, T. Taniguchi, C. Volk, and C. Stampfer, Spin relaxation in a single-electron graphene quantum dot, Nat. Commun. **13**, 3637 (2022).

[18] S. Möller, L. Banszerus, A. Knothe, C. Steiner, E. Icking, S. Trellenkamp, F. Lentz, K. Watanabe, T. Taniguchi, L. I. Glazman, V. I. Fal'ko, C. Volk, and C. Stampfer, Probing two-electron multiplets in bilayer graphene quantum dots, Phys. Rev. Lett. **127**, 256802 (2021).

[19] C. Tong, F. Ginzel, W. W. Huang, A. Kurzmann, R. Garreis, K. Watanabe, T. Taniguchi, G. Burkard, J. Danon, T. Ihn, and K. Ensslin, Three-carrier spin blockade and coupling in bilayer graphene double quantum dots, arXiv:2211.04882.

[20] R. Garreis, C. Tong, J. Terle, M. J. Ruckriegel, J. D. Gerber, L. M. Gächter, K. Watanabe, T. Taniguchi, T. Ihn, K. Ensslin, and W. W. Huang, Long-lived valley states in bilayer graphene quantum dots, arXiv:2304.00980.

[21] L. Banszerus, S. Möller, K. Hecker, E. Icking, K. Watanabe, T. Taniguchi, F. Hassler, C. Volk, and C. Stampfer, Particle–hole symmetry protects spin-valley blockade in graphene quantum dots, Nature (London) **618**, 51 (2023).

[22] P. Stano and D. Loss, Review of performance metrics of spin qubits in gated semiconducting nanostructures, Nat. Rev. Phys. **4**, 672 (2022).

[23] A. Knothe and V. Fal'ko, Influence of minivalleys and Berry curvature on electrostatically induced quantum wires in gapped bilayer graphene, Phys. Rev. B **98**, 155435 (2018).

[24] C. Moulsdale, A. Knothe, and V. Fal'ko, Engineering of the topological magnetic moment of electrons in bilayer graphene using strain and electrical bias, Phys. Rev. B **101**, 085118 (2020).

[25] A. Knothe and V. Fal'ko, Quartet states in two-electron quantum dots in bilayer graphene, Phys. Rev. B **101**, 235423 (2020).

[26] A. Knothe, L. I. Glazman, and V. Fal'ko, Tunneling theory for a bilayer graphene quantum dot's single-and two-electron states, New J. Phys. **24**, 043003 (2022).

[27] J. R. Petta, A. C. Johnson, J. M. Taylor, E. A. Laird, A. Yacoby, M. D. Lukin, C. M. Marcus, M. P. Hanson, and A. C. Gossard, Coherent manipulation of coupled electron spins in semiconductor quantum dots, Science **309**, 2180 (2005).

[28] F. H. Koppens, J. A. Folk, J. M. Elzerman, R. Hanson, L. W. Van Beveren, I. T. Vink, H.-P. Tranitz, W. Wegscheider, L. P. Kouwenhoven, and L. M. Vandersypen, Control and detection

of singlet-triplet mixing in a random nuclear field, Science **309**, 1346 (2005).

[29] A. Johnson, J. Petta, J. Taylor, A. Yacoby, M. Lukin, C. Marcus, M. Hanson, and A. Gossard, Triplet–singlet spin relaxation via nuclei in a double quantum dot, Nature (London) **435**, 925 (2005).

[30] C. Barthel, D. J. Reilly, C. M. Marcus, M. P. Hanson, and A. C. Gossard, Rapid single-shot measurement of a singlet-triplet qubit, Phys. Rev. Lett. **103**, 160503 (2009).

[31] J. R. Prance, Z. Shi, C. B. Simmons, D. E. Savage, M. G. Lagally, L. R. Schreiber, L. M. K. Vandersypen, M. Friesen, R. Joynt, S. N. Coppersmith, and M. A. Eriksson, Single-shot measurement of triplet-singlet relaxation in a Si/SiGe double quantum dot, Phys. Rev. Lett. **108**, 046808 (2012).

[32] A. C. Johnson, J. R. Petta, C. M. Marcus, M. P. Hanson, and A. C. Gossard, Singlet-triplet spin blockade and charge sensing in a few-electron double quantum dot, Phys. Rev. B **72**, 165308 (2005).

[33] X. Cai, E. J. Connors, L. F. Edge, and J. M. Nichol, Coherent spin–valley oscillations in silicon, Nat. Phys. **19**, 386 (2023).

[34] T. Ohta, A. Bostwick, T. Seyller, K. Horn, and E. Rotenberg, Controlling the electronic structure of bilayer graphene, Science **313**, 951 (2006).

[35] E. McCann, Asymmetry gap in the electronic band structure of bilayer graphene, Phys. Rev. B **74**, 161403(R) (2006).

[36] J. B. Oostinga, H. B. Heersche, X. Liu, A. F. Morpurgo, and L. M. Vandersypen, Gate-induced insulating state in bilayer graphene devices, Nat. Mater. **7**, 151 (2008).

[37] See Supplemental Material at http://link.aps.org/supplemental/10.1103/PhysRevResearch.6.L012006 for discussions on (S1) methods, describing details on sample fabrication and geometry, tuning parameters, and the Coloumb diamonds at which the Kondo measurements were taken, and (S2) magnetospectroscopy along DQD detuning lines, describing the analysis of relevant states and transitions near (1,2)–(0,3), (1,3)–(0,4), and (2,2)–(1,3) charge degeneracies in an external perpendicular magnetic field [50,51].

[38] C. L. Kane and E. J. Mele, Quantum spin Hall effect in graphene, Phys. Rev. Lett. **95**, 226801 (2005).

[39] S. Konschuh, M. Gmitra, D. Kochan, and J. Fabian, Theory of spin-orbit coupling in bilayer graphene, Phys. Rev. B **85**, 115423 (2012).

[40] G. Y. Wu, N.-Y. Lue, and Y.-C. Chen, Quantum manipulation of valleys in bilayer graphene, Phys. Rev. B **88**, 125422 (2013).

[41] E. A. Laird, J. M. Taylor, D. P. DiVincenzo, C. M. Marcus, M. P. Hanson, and A. C. Gossard, Coherent spin manipulation in an exchange-only qubit, Phys. Rev. B **82**, 075403 (2010).

[42] B.-B. Chen, B.-C. Wang, G. Cao, H.-O. Li, M. Xiao, G.-C. Guo, H.-W. Jiang, X. Hu, and G.-P. Guo, Spin blockade and coherent dynamics of high-spin states in a three-electron double quantum dot, Phys. Rev. B **95**, 035408 (2017).

[43] D. Goldhaber-Gordon, H. Shtrikman, D. Mahalu, D. Abusch-Magder, U. Meirav, and M. Kastner, Kondo effect in a single-electron transistor, Nature (London) **391**, 156 (1998).

[44] J. Kondo, Resistance minimum in dilute magnetic alloys, Prog. Theor. Phys. **32**, 37 (1964).

[45] K. G. Wilson, The renormalization group: Critical phenomena and the Kondo problem, Rev. Mod. Phys. **47**, 773 (1975).

[46] S. M. Cronenwett, T. H. Oosterkamp, and L. P. Kouwenhoven, A tunable Kondo effect in quantum dots, Science **281**, 540 (1998).

[47] W. Van der Wiel, S. D. Franceschi, T. Fujisawa, J. Elzerman, S. Tarucha, and L. Kouwenhoven, The Kondo effect in the unitary limit, Science **289**, 2105 (2000).

[48] J. Nygård, D. H. Cobden, and P. E. Lindelof, Kondo physics in carbon nanotubes, Nature (London) **408**, 342 (2000).

[49] doi:10.3929/ethz-b-000645963.

[50] H. Overweg, H. Eggimann, X. Chen, S. Slizovskiy, M. Eich, R. Pisoni, Y. Lee, P. Rickhaus, K. Watanabe, T. Taniguchi *et al.*, Electrostatically induced quantum point contacts in bilayer graphene, Nano Lett. **18**, 553 (2018).

[51] L. Wang, I. Meric, P. Huang, Q. Gao, Y. Gao, H. Tran, T. Taniguchi, K. Watanabe, L. Campos, D. Muller *et al.*, One-dimensional electrical contact to a two-dimensional material, Science **342**, 614 (2013).